Version of Record: https://www.sciencedirect.com/science/article/pii/S0967064516300996
Manuscript_809414d14c09286e99051e2017a6c92e

Patterns of Upwelling and Relaxation around Monterey Bay based on Long-Term Observations of Surface Currents from High Frequency Radar

Jeffrey D. Paduan[1], Michael S. Cook[1], and V. Mario Tapia[2]

ABSTRACT

A five-year record of surface current observations from HF radar in the region around Monterey Bay are used to describe the dominant circulation patterns under upwelling- and downwelling-favorable wind forcing. Conditional averages based on local wind observations reveal more structure and intensity in the circulation patterns than do traditional temporal averages. The predominant upwelling circulation pattern in the region is found to reach full strength after about three days of persistent upwelling-favorable wind forcing. In the opposite phase under downwelling-favorable winds, the circulation patterns differ between summer and winter with evidence for strong connectivity between the offshore waters and the coastline around Monterey Bay in summer that is not present in winter.

1. INTRODUCTION

Surface currents affect many critical processes in the coastal ocean, such as dispersal of harmful material accidentally spilled into the water or larvae that spend part of their life in the surface flow. Over the past twenty years, a method of remotely sensing ocean surface currents using shore-based, high frequency (HF) radar systems has been developed and deployed along much of the California coastline (Paduan et al., 2004). In the HF radiowave band, signals are resonantly backscattered by ocean surface waves having exactly ½ the physical wavelength of the transmitted radiowave through the process of Bragg scattering (Crombie, 1955; Barrick and Webber, 1970). Present-day HF radar systems exploit this resonance phenomenon to map ocean surface currents on hourly time scales out to distances of about 100 km offshore. The horizontal resolution of the measurements varies with the specific frequency and bandwidth configuration, but is typically a few kilometers. The many uses of HF radar-derived surface current observations have been reviewed in the article by Paduan and Washburn (2013). In this paper, we focus on recurring circulation patterns seen in long-term HF radar observations near Monterey Bay, California.

The region in and around Monterey Bay in central California has been the site of HF radar observations of ocean surface currents dating back to the early 1990s (e.g., Petruncio, 1993; Paduan and Rosenfeld, 1996; Paduan and Graber, 1997; Paduan and Cook, 1997; Lipphardt et al., 2006; Kaplan et al., 2009;). In addition, the region has enjoyed continuous observations at deep-ocean mooring sites supported by the Monterey Bay Aquarium Research Institute (MBARI; Chavez et al., 1997) as well as the National Weather Service (see: http://www.ndbc.noaa.gov). Ocean observations, such as the surface current mapping by HF radar and the wind and subsurface velocity, temperature, and salinity observations at the mooring sites, are important because of the information they provide about coastal upwelling processes.

[1] Department of Oceanography, Naval Postgraduate School, Monterey CA 93943
[2] University of Santa Clara, Santa Clara, CA 95053

These processes are critical influences on the coastal ocean ecology and weather along central California. The prevalence of upwelling makes the region one of the most productive anywhere (Chavez and Messié, 2009). For this reason, upwelling processes have been the focus of many in situ experiments and modeling efforts (e.g., Ramp et al., 2008). In contrast with the early textbook view of upwelling as a two-dimensional process, modern observations reveal it to be three dimensional with concentrated upwelling centers associated, usually, with major headlands. This new paradigm was established by the advent of satellite observations of ocean surface temperatures and ocean color (Ikeda and Emery, 1984; Abbott and Barksdale, 1991). The earliest versions of observations motivated a series of field experiments along the U.S. west coast that verified the fact that the filamentary structures of order 10 km width observed by satellites are, indeed, related to dynamical features in the circulation and parallel structure in the ecological parameters (Brink and Cowles, 1991; Brink et al., 1991; Washburn et al., 1991; Brink et al., 2000).

Many past experiments in Monterey Bay have focused on the upwelling plume and associated front that is observed to originate immediately north of the Bay in response to upwelling favorable wind forcing (Figure 1; Ryan et al., 2008, Ryan et al., 2009; Woodson et al., 2009; Ryan et al., 2010). These studies motivate the present analyses in that they suggest recurring dynamical features tied to the coastline morphology around Monterey Bay. HF radar-derived surface currents are expected to reflect these dynamical features.

The combination of long records of surface current mapping data and the patchy yet repeating nature of upwelling in the Monterey Bay area provide motivation for a retrospective analysis along the lines of the earlier work by Enriquez (2004). Given the known connections between upwelling and productivity and between upwelling fronts and concentrated productivity, describing the repeating pattern of upwelling circulation will identify the critical features for this region. Furthermore, relating the features around Monterey Bay with similar features throughout the California Current System should allow local to be exported to other locations. To the extent that upwelling circulation patterns are found to be recurring, their presence also becomes predictable. This, in turn, can be used in real-time responses to transportation issues, such as the movement of spilled oil, or in ecological modeling, such as the prediction of larval transport pathways. In this paper, we look at a multi-year record of surface current observations in an effort to reveal these recurring circulation patterns. We focus on the five-year period 2006 through 2010, which includes the best existing HF radar coverage. Section 2 describes the data set and the conditional averaging approach applied to the data. Section 3 presents the results in terms of the recurring patterns of upwelling- and relaxation-period surface currents for the summer and winter seasons and Section 4 presents a summary and conclusions.

2. DATA AND METHODS

As mentioned in Section 1, the region around Monterey Bay, California has some of the longest records of surface current observations from HF radar systems anywhere. The spatial coverage available in the historical data set is not, however, uniform. Early on, the observations were primarily within the Bay. Beginning in 2004, the State of California funded a major expansion of the existing HF radar systems to create a state-wide network as part of the Coastal Ocean Currents Monitoring Program (COCMP). Operation of that network peaked in 2010. After that

time, operations and maintenance responsibility for the network shifted to NOAA's Integrated Ocean Observing Network (IOOS), which continues to operate HF radar networks nationwide. Funding available under IOOS is not, however, adequate to maintain the previous density and extent of observations offshore California.

In the region of central California, HF radar surface current observations were most plentiful during the five-year period from 2006 through 2010. Other studies have analyzed these data for regional (e.g., Kaplan et al., 2009) or coast-wide (e.g., Kim et al., 2011) insights. Here, the focus is on describing the surface velocity patterns associated with the individual upwelling centers near Monterey Bay. Spatial availability of the hourly surface current observations used in this study is shown on Figure 2 together with the locations of the contributing HF radar stations and the offshore mooring #46042. The offshore extent of the coverage greatly exceeds previous studies using the Monterey Bay area HF radar data, such as the early work of Paduan and Rosenfeld (1996) and the thesis work of Enriquez (2004). The latter work serves as a template for the present study. In both cases, patterns of upwelling circulation are revealed using conditional averaging of the surface current observations based on independent observations of surface winds.

Conditional averaging as used here would be defined more formally as a type of conditional expectation or joint probability distribution within the probability theory literature (e.g., Grinstead and Snell, 1997). Key here is the a priori assumption that alongshore wind stress is the primary driver of upwelling circulation. Many previous studies have illustrated how HF radar-derived surface currents are highly responsive to local wind, particularly at high frequencies (e.g., Paduan and Rosenfeld, 1996; Paduan and Cook, 1997; Ramp et al., 2005; Kohut et al., 2006). Given this background, it is obvious that averaged currents formed around common wind forcing conditions associated with upwelling are more likely to represent the spatial surface current patterns associated with upwelling than are other types of averaged currents, such as those formed strictly on the basis of season. This analysis approach does not rule out the impact of geostrophic currents but those flows are large scale and slowly varying compared with the responses to episodic upwelling wind forcing.

For the central California coastal area, upwelling-favorable winds are the most common; the second most common wind direction in the region is the opposite direction, i.e., downwelling-favorable winds that blow along the coast toward the northwest (Figure 3). Enriquez (2004) showed that both wind direction and persistence are important in determining the resulting patterns of upwelling or downwelling circulation in Monterey Bay. Here we follow that lead with the additional goal to characterize the spin-up time required for upwelling circulation to reach quasi steady state.

In this study, we use 33 hour low-pass-filtered wind observations, sampled hourly, from mooring #46042 as the independent indicator of forcing status, e.g., upwelling-favorable versus downwelling-favorable winds. The winds are paired with similarly filtered surface current data. Filtering the wind and current data can be expected to reduce the fidelity of the targeted upwelling circulation pattern to some degree. It is necessary, however, because of the significant tidal-period energy that is present in the surface currents and diurnal period energy that is present in the winds in this region (Paduan and Cook, 1997). The number of ensemble members (i.e.,

events) present in the conditional averages presented here were deemed to be too few to insure that these diurnal- and semi-diurnal-period fluctuations would be eliminated by the conditional average itself despite the five-year record length.

Several general characterizations can be made about coastal winds offshore central California in addition to the predominant direction illustrated in Figure 3. Firstly, it is the case that upwelling-favorable winds are the most common winds in both summer and winter. The persistence of upwelling winds, however, varies dramatically between the seasons as illustrated in Figure 4. In summer, upwelling events are longer with typically several days of upwelling-favorable wind interrupted by just a few days of wind relaxation or, in some cases, weak wind reversals. In winter, upwelling-favorable wind events are shorter and the intervening downwelling-favorable wind events are both longer in duration and stronger than in summer.

The concept of conditional averaging is also illustrated in Figure 4, including the spin-up time parameter. In this example, bold vectors in the winter data represent hours for which the speed exceeded 5.0 m/sec, the direction originated from between 280 degrees and 330 degrees, and these joint conditions were satisfied for, at least, the preceding 12 hours (i.e., the prescribed spin-up time). Applying those conditional averaging parameters over the 2006-2007 winter season shown in Figure 4, the conditional average wind speed for upwelling-favorable winds was 10.2 m/sec and the direction was 296 degrees. By contrast, the traditional three-month average yields a winter average wind speed of only 2.7 m/sec and average direction of 292 degrees because of the many offsetting periods of downwelling-favorable winds that are included in that seasonal average. This illustration of the conditional averaging process is relevant throughout this work. The key parameters for selecting data points from the surface current records based on the wind conditions are the speed of the wind, both lower and upper bounds, the direction of the wind, both left and right bounds, and the duration of the winds. The duration parameter controls the length of time that the wind speed and direction criteria must be met *before* the surface current data begin accumulating, which allows for a variable spin-up time.

The goal to characterize the spin-up time required for upwelling circulation to reach quasi steady state was approached by computing the mean kinetic energy of the observed surface currents within different sub regions of the HF radar observation domain. The results below focus on the mean kinetic energy observed in the sub domain offshore of the Monterey Peninsula as shown in Figure 2. The mean kinetic energy at a given time is defined simply as the spatial average of the kinetic energy at each individual HF radar observation point, i.e.:

$$\langle KE \rangle = \frac{1}{n}\sum_{i=1}^{n}\frac{1}{2}(u_i^2 + v_i^2). \quad (1)$$

3. RESULTS

A clear example of the difference between the surface current patterns resulting from a traditional average by season and a conditional average based on independent wind conditions is seen in the comparison between Figure 5 and Figure 6. In Figure 5, the summer average surface currents are shown based on the observations from the five summers from 2006 through 2010 where summer includes data from May through September. By comparison, Figure 6 shows the conditionally averaged surface currents during upwelling favorable wind conditions with a spin-

up time of 8 ½ days. While the familiar pattern of equatorward flow offshore and cyclonic flow within Monterey Bay is present in both results, the flow intensity is much greater in the conditionally averaged result. Given that the conditionally averaged upwelling circulation pattern in Figure 6 is based on 12 separate events over five summers, it is assumed to be a robust representation of the fully developed upwelling circulation in the Monterey Bay region. This assumption is supported by the generally small size of the standard error vectors also shown in Figure 6, which were computed assuming that each of the 12 sampled events provided an independent realization of the pattern.

The upwelling circulation pattern in Figure 6 is based on a long spin-up time in excess of a week. By varying the requisite spin-up time in the conditional averaging process, it is possible to estimate how long is required for the upwelling circulation in the Monterey Bay region to become fully developed. To answer that question, we varied the spin-up time between 12 hours and 216 hours in 12-hour increments. A representation of the strength of the circulation pattern under different spin-up conditions is shown in Figure 7, which presents the mean kinetic energy in the test region shown on Figure 2 using Equation (1) as a function of spin-up time. The particular test region used is arbitrary but it was chosen to encompass a portion of the strong flow of the upwelling jet that forms off the mouth of Monterey Bay. Based on this metric, it appears that the upwelling circulation in the Monterey Bay region becomes fully developed after about three days of persistent upwelling-favorable winds.

An alternative visualization of the fully developed upwelling circulation in the Monterey Bay region is shown in Figure 8, which presents example trajectories that would result from this flow were it frozen over time. In this example, surface particles have been deployed at the northern end of the domain and at positions within Monterey Bay. The pattern indicates a nominal separation of the offshore and inshore flow separated, approximately, by those trajectories that intersect Point Pinos, which is at the northwest tip of the Monterey peninsula (Figure 2). In the upwelling case, the trajectories for the traditional seasonally averaged summertime circulation pattern (not shown) are similar to those in Figure 8 but with movements that are two or three times slower. We also reviewed the circulation patterns revealed by conditionally averaging the observed surface currents during upwelling wind conditions but with shorter spin-up times. It turns out that the pattern is consistent in all cases; only the intensity increases as the spin-up time is lengthened between one day and nine days.

While the upwelling circulation patterns revealed here are associated with nutrient supply and high productivity, the opposite-phase patterns during downwelling-favorable wind conditions may also be associated with important ecological events. It has long been hypothesized that the less common downwelling events are critical for bringing surface waters onto or close to the shoreline (Wing et al., 1995; Graham and Largier, 1997). Such physical drivers are, in turn, assumed to be responsible for allowing larvae of intertidal aquatic species to recruit to the shoreline as well as for bringing oil or other pollutants onto the shoreline.

The conditionally averaged circulation patterns during downwelling-favorable wind conditions are shown, separately, in Figure 9 for winter months and in Figure 10 for summer months. Here a shorter spin-up time of 24 hours is used because downwelling events are not observed to persist as long as upwelling events. In addition, these patterns are the result of wind forcing in the 4-8

m/sec range as opposed to selecting everything greater than 4 m/sec. This was done in order to select similar forcing between the two seasons. Winds greater than 8 m/sec are rare in summer but occur with some frequency in winter. The resulting downwelling patterns are qualitatively similar between winter and summer with poleward flow offshore and a cyclonic circulation pattern within Monterey Bay. Flow is strongest in the south and across the mouth of Monterey Bay, particularly in the wintertime example. There is evidence of flow toward the coast to the south of Monterey Bay and in southern Monterey Bay in both seasons.

The frozen-field visualizations for both the winter and summer downwelling circulation patterns are shown in Figure 11. In this view, there are obvious and potentially significant differences between the results for the two seasons: while there is strong evidence of connectivity between the offshore flow and Monterey Bay during summer downwelling events, there is no clear evidence of a similar connectivity during winter downwelling events. This summertime transport of water onto the coast during downwelling conditions is consistent with observations along the coastline (e.g., Bjorkstedt and Roughgarden, 1997). It should be noted that our observations miss potentially important pathways very near the coastline. Still there does appear to be a difference in the level of connectivity via the mean currents between summer and winter.

The spatial information derived from the HF radar observations provides a unique view of the processes related to upwelling and downwelling conditions. It is possible, for example, to compute the horizontal divergence of the derived circulation patterns. Here we present those results for the various upwelling and downwelling conditions reviewed above (Figure 12 and Figure 13). Divergence computations for geophysical flow fields in the ocean are easy to conduct if spatial information is available but they are difficult to assess. Oceanographic flows always have low absolute values of divergence composed from the summation of two much larger components. Hence, in the presence of measurement error, the uncertainty of the divergence computation is high. The results in Figure 12 and Figure 13 were produced from the two-dimensional surface current patterns using a horizontal smoothing (i.e., independence) scale of around 10 km. Despite the large uncertainty in these numbers, there is evidence for divergence (i.e., upwelling) along and offshore of the main jet crossing Monterey Bay during upwelling conditions (Figure 13) with a magnitude around 25% of the local Coriolis parameter. During the comparable downwelling conditions that divergence region disappears with some hint of a change in sign. Of all of the examples here, the patterns during wintertime downwelling exhibit the clearest physical interpretation appearing as alternative bands of positive and negative divergence parallel to the main current axis.

4. CONCLUSIONS

Using a five-year record of surface current mapping data from HF radar observations around Monterey Bay, we contrast the patterns resulting from traditional temporal averaging with those resulting from conditional averages based on local wind observations. Not surprisingly, the pattern of upwelling-related circulation is stronger and better defined when averages are based on only those hours during which upwelling-favorable wind conditions existed. Because of the common wind (and current) reversals in the region, averages by month or by season produce weak results.

Because the upwelling circulation pattern is wind driven and also influenced by the shape of the coastline, upwelling jets tend to appear in the same locations. The jets are observed to strengthen with time under the influence of steady, upwelling-favorable winds. That strengthening does not, however, continue indefinitely. Results here suggest that the circulation pattern comes into equilibrium with its surroundings in the Monterey Bay region after about three days of upwelling-favorable wind forcing. What is surprising about the canonical upwelling circulation pattern presented here is the apparent lack of connection—via the mean currents—between the upwelling source waters north of Monterey Bay and the Bay itself. Ecological and remote sensing observations (e.g., Rosenfeld et al., 1994; Paduan and Rosenfeld, 1996; Graham and Largier, 1997), along with the long standing recognition of relatively high productivity in Monterey Bay, seem to contradict the surface current results presented here. Either the analysis used here has obscured the direct pathway between the upwelling source waters and Monterey Bay or there is a vigorous mixing of properties across the mean velocity pathways that delivers significant amounts of cold, nutrient-rich waters into the Monterey Bay circulation pattern.

Downwelling-favorable wind forcing also produces distinct and important circulation patterns, although they are reproduced less precisely than are the patterns driven by upwelling-favorable wind forcing. This is, perhaps, because downwelling-favorable wind events persist over much shorter periods. It is also shown in this study, however, that there is a systematic difference in the downwelling circulation patterns between summer and winter for the Monterey Bay region. These findings may be ecologically significant in that they indicate a clear connection between offshore waters and the Monterey Bay coastline during summertime downwelling events. Such a connection is missing or less certain during wintertime downwelling events. Downwelling wind event forcing does differ in strength and duration between winter and summer (e.g., Figure 4). Future studies should attempt to detangle whether or not wind variations alone can explain the differences observed in downwelling circulation patterns between seasons or whether additional factors, such as differences in vertical shear between seasons, are required to explain them.

We expect that differences in the initial conditions of the three dimensional density field have more to do with controlling the downwelling circulation patterns than they do with the upwelling circulation patterns. This is because downwelling is more precisely described as a relaxation process. Often the wind forcing is weak yet the current pattern still reverses implying a role for the alongcoast pressure gradient.

Acknowledgments

This work was supported by NOAA's Integrated Ocean Observing System (IOOS) program through its Central and Northern California Ocean Observing System (CeNCOOS) regional association and award number NA11NOS0120032. V Tapia was supported by the National Science Foundation's Research Experience for Undergraduates (REU) program through California State University Monterey Bay and hosted at the Naval Postgraduate School.

REFERENCES

Abbott, M.R., and B. Barksdale, 1991: Phytoplankton pigment patterns and wind forcing off central California. *J. Geophys. Res*., **96**, 14649-14667.

Bjorkstedt, E., and J. Roughgarden, 1997: Larval transport and coastal upwelling: an application of HF radar in ecological research. *Oceanography*, **10**, 64-67.

Brink, K.H., and T.J. Cowles, 1991: The Coastal Transition Zone Program. *J. Geophys. Res*., **96**, 14637-14647.

Brink, K.H., R.C. Beardsley, P.P. Niiler, M. Abbott, A. Huyer, S. Ramp, T. Stanton, and D. Stuart, 1991: Statistical properties of near-surface flow in the California Coastal Transition Zone. *J. Geophys., Res*., **96**, 14693-14706.

Brink, K.H., R.C. Beardsley, J.D. Paduan, R. Limeburner, M. Caruso, and J.G. Sires, 2000: A view of the 1993-1994 California Current based on surface drifters, RAFOS floats, and remotely sensed data. *J. Geophys. Res*., **105**, 8575-8604.

Chavez, F. P., and Messié, M., 2009: A comparison of eastern boundary upwelling ecosystems. *Progress in Oceanography*, **83**, 80–96.

Chavez, F.P., J.T. Pennington, R. Herlien, H. Jannasch, G. Thurmond, G.E. Friederich, 1997: Moorings and drifters for real-time interdisciplinary oceanography. *J.Atm. Ocean. Technology*, **14**, 1119-1211.

Enriquez, A., 2004: An investigation of surface current patterns related to upwelling in Monterey Bay using high frequency radar. M.S. Thesis, Naval Postgraduate School, Monterey, CA, June, 83pp.

Graham, W.M., and J.L. Largier, 1997: Upwelling shadows as nearshore retention sites: the example of northern Monterey Bay. *Cont. Shelf Res*., **17**, 509-532.

Grinstead, C.M., and J.L. Snell, 1997: *Introduction to Probability*. American Mathematical Society, Providence, Rhode Island, 510 pp.

Ikeda, M., and W.J. Emery, 1984: Satellite observations and modeling of meanders in the California Current System off Oregon and northern California. *J. Phys. Oceanogr*., **14**, 1434-1450.

Kaplan, D. M., C. Halle, J. Paduan, and J. L. Largier, 2009: Surface currents during anomalous upwelling seasons off central California. *J. Geophys. Res*., doi:10.1029/2009JC005382.

Kim, S.Y., E.J. Terrill, B.D. Cornuelle, B.Jones, L. Washburn, M.A. Moline, J.D. Paduan, N. Garfield, J. Largier, G. Crawford, and P.M. Kosro, 2011: Observations of high-resolution coastal surface circulation on the U. S. West Coast. *J. Geophys. Res*., **116**, C03011, doi:10.1029/2010JC006669.

Kohut, J.T., S.M. Glenn, and J.D. Paduan, 2006: Inner-shelf response to tropical storm Floyd. *J. Geophys. Res*., **111**, c09S91, doi:10.1029/2003JC002173.

Lipphardt, B.L., Jr., D. Small, A.D. Kirwan, Jr., W. Wiggins, K. Ide, C.E. Grosch, and J.D. Paduan, 2006: Synoptic Lagrangian maps: Application to surface transport in Monterey Bay. *J. Mar. Res*., **64**(2), 221-247.

Paduan, J.D., and M.S. Cook, 1997: Mapping surface currents in Monterey Bay with CODAR-type HF radar. *Oceanography*, **10**, 49-52.

Paduan, J.D., and H.C. Graber, 1997: Introduction to high frequency radar: Reality and myth. *Oceanography*, **10**, 36-39.

Paduan, J.D., P.-M. Kosro, and S.M. Glenn, 2004: A national coastal ocean surface current mapping system for the United States. *Marine Tech. Soc*., **38**, 102-108.

Paduan, J.D., and L.K. Rosenfeld, 1996: Remotely sensed surface currents in Monterey Bay from shore-based HF radar (CODAR). *J. Geophys. Res.*, **101**, 20669-20686.

Paduan, J.D., and L. Washburn, 2013: High-frequency radar observations of ocean surface currents. *Annu. Rev. Mar. Sci*., **5**, 115–136.

Petruncio, E.T., 1993: Characterization of tidal currents in Monterey Bay from remote and in situ measurements. M.S. thesis, Department of Oceanography, Naval Postgraduate School, 113 pp.

Ramp, S.R., J.D. Paduan, I. Shulman, J. Kindle, F.L. Bahr, and F.P. Chavez, 2005: Observations of upwelling and relaxation events in the northern Monterey Bay during August 2000. *J. Geophys. Res*., **110**, C07013, doi:10.1029/2004JC002538.

Ramp, S.R., R.E. Davis, N.E. Leonard, I. Shulman, Y. Chao, A.R. Robinson, J. Marsden, P.F.J. Lermusiaux, D. Fratantoni, J.D. Paduan, F.P. Chavez, F.L. Bahr, S. Liang, W. Leslie, and Z. Li, 2008: Preparing to predict: The Second Autonomous Ocean Sampling Network (AOSN-II) experiment in the Monterey Bay. *Deep-Sea Res*., doi:10.1016/j.dsr2.2008.08.013.

Rosenfeld, L.K., Schwing, F.B., Garfield, N., Tracy, D.E., 1994. Bifurcated flow from an upwelling center: a cold water source for Monterey Bay. *Continental Shelf Research*, **14,** 931–964.

Ryan, J.P., M.A. McManus, J.D. Paduan, and F.P. Chavez, 2008: Phytoplankton thin layers caused by shear in frontal zones of a coastal upwelling system. *Mar. Ecology Prog. Series*, **354**, doi: 10.3354/meps07222.

Ryan, J.P., A.M. Fischer, R.M. Kudela, J.F.R. Gower, S.A. King, R. Marin III, and F.P. Chavez, 2009: Influences of upwelling and downwelling winds on red tide bloom dynamics in Monterey Bay, California. *Cont. Shelf Re*s., **29**, doi:10.1016/j.csr.2008.11.006.

Ryan, J.P., A.M. Fischer, R. M. Kudela, M.A. McManus, J.S. Myers, J.D. Paduan, C.M. Ruhsam, C.B. Woodson, and Y. Zhang, 2010: Recurrent frontal slicks of a coastal ocean upwelling shadow. *J. Geophys. Res*., **115**, C12070, doi:10.1029/2010JC006398.

Washburn, L., D.C. Kadko, B.H. Jones, T. Hayward, P.M. Kosro, T.P. Stanton, S. Ramp, and T. Cowles, 1991: Water mass subduction and the transport of phytoplankton in a coastal upwelling system. *J. Geophys. Res*., **96**, 14927-14945.

Wing, S.R., J.L. Largier, L.W. Botsford, and J.F. Quinn, 1995: Settlement and transport of benthic invertebrates in an intermittent upwelling region. *Limnol. & Oceanogr*., **40**, 316-329.

Woodson, C.B., L. Washburn, J.A. Barth, D.J. Hoover, A.R. Kirincich, M.A. McManus, J.P. Ryan, and J. Tyburczy, 2009: Northern Monterey Bay upwelling shadow front: Observations of a coastally and surface-trapped buoyant plume. J. Geophys. Res., 114, C12013, doi:10.1029/2009JC005623.

FIGURE CAPTIONS

Figure 1. Satellite-derived sea surface temperature (˚C) on 15 April 2016 from NOAA's CoastWatch program as supported by the National Weather Service Monterey Forecast Office.

Figure 2. Locations of hourly surface current observations and their percent coverage during the period 2006 through 2010. Locations with less than 75% temporal coverage (further indicated by an X) were not used in this study. Locations of contributing coastal HF radar sites and the location of NOAA's offshore mooring #46042 are marked by triangles and a circle, respectively. The HF radar locations are, from north-to-south, at Santa Cruz (SCRZ), Moss Landing (MLML), Naval Postgraduate School, Monterey (NPGS), Point Pinos (PPIN), Granite Canyon (GCYN), and Point Sur (PSUR). Note: At least, two additional HF radar sites located to the north of the mapping domain also contributed to vector current mapping within the domain. The bounding box in the southeast portion of the domain encloses the grid points whose kinetic energy is averaged together as an indication of the strength of the upwelling circulation. Representative depth contours (m) are also shown.

Figure 3. Directional statistics of 43,331 hourly wind velocity observations (out of a possible 43,824 hours) for the period 2006 through 2010 at NOAA's mooring #46042.

Figure 4. Sample summer (upper) and winter (lower) wind velocity at mooring #46042. Bold vectors in the winter data represent hours for which the speed exceeded 5.0 m/sec, the direction originated from between 280 degrees and 330 degrees, and these joint conditions were satisfied for, at least, the preceding 12 hours.

Figure 5. Summer (May-September) seasonal average surface currents and winds for 2006 through 2010. Representative depth contours (m) are also shown.

Figure 6. Upwelling circulation pattern for the summer months of May-September for 2006 through 2010 with wind speeds greater than 5.0 m/sec, wind direction between 280 degrees and 325 degrees, and these joint conditions having been met for between 204 hours to 216 hours (a spin up time of 8 ½ days). These upwelling-favorable wind conditions were matched 127 times in 12 events. The conditional average circulation pattern (upper) is paired with the standard error pattern (lower) assuming each event was independent. Representative depth contours (m) are also shown.

Figure 7. Mean kinetic energy within the sub grid area on Figure 2 as a function of time since the onset of upwelling-favorable winds.

Figure 8. Frozen field visualization of the fully developed upwelling circulation pattern shown in Figure 5. X locations indicate the starting positions of offshore (blue) and inshore (green) surface particles.

Figure 9. Circulation patterns during downwelling-favorable wind forcing with wind speeds >4 m/sec but <8 m/sec, wind direction from between 90 degrees and 150 degrees, and these joint conditions having been in place for, at least, 24 hours for the winter months of December, January, and February. These downwelling-favorable wind conditions were matched 57 times in 5 events. The conditional average circulation pattern (upper) is paired with the standard error

pattern (lower) assuming each event was independent. Representative depth contours (m) are also shown.

Figure 10. Circulation patterns during downwelling-favorable wind forcing with wind speeds >4 m/sec but <8 m/sec, wind direction from between 90 degrees and 135 degrees, and these joint conditions having been in place for, at least, 24 hours for the spring and summer months of May through September. The downwelling-favorable wind conditions were matched 65 times in 6 events. The conditional average circulation pattern (upper) is paired with the standard error pattern (lower) assuming each event was independent. Representative depth contours (m) are also shown.

Figure 11. Frozen field visualization of the fully developed downwelling circulation patterns shown in Figure 9 and Figure 10 for winter (left) and spring-summer (right), respectively.

Figure 12. Convergence (sec^{-1}) for the wintertime (left) and summertime (right) downwelling circulation patterns from Figure 10. Representative depth contours (m) are also shown.

Figure 13. Convergence (sec^{-1}) for the fully developed summertime upwelling circulation pattern from Figure 6. Representative depth contours (m) are also shown.

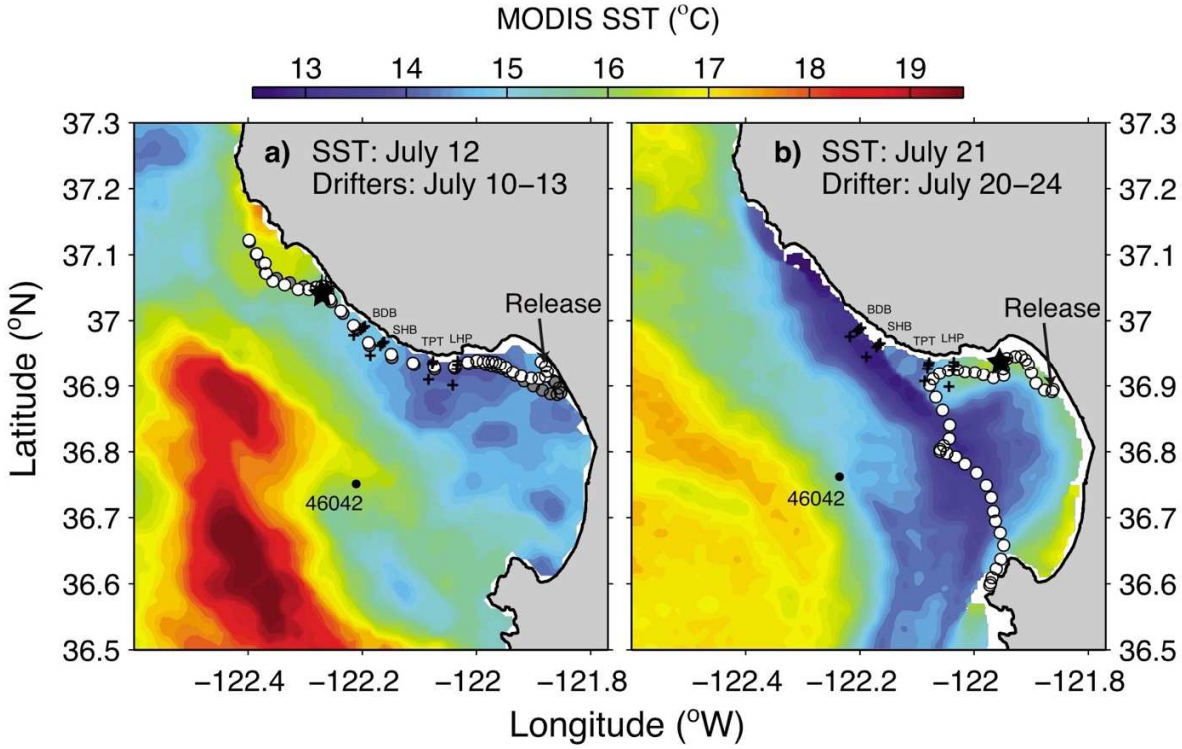

Figure 1. Sea surface temperatures (MODIS) and drifter tracks during (a) relaxation and (b) upwelling. Plus indicates mooring locations for current study. Star indicates location of drifters on date of satellite image shown. Locations (circles) are regularly spaced in time in order to provide relative speeds (from Woodson et al., 2009).

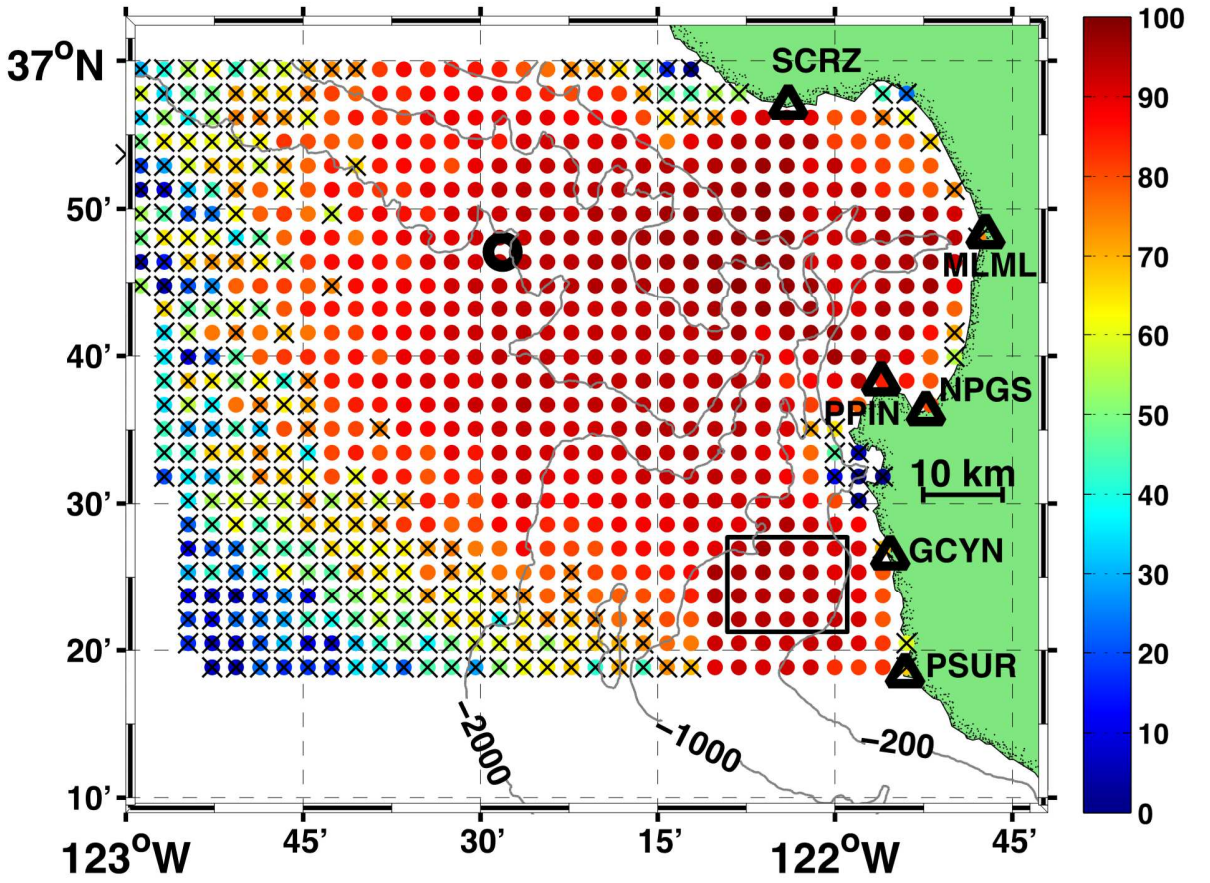

Figure 2. Locations of hourly surface current observations and their percent coverage during the period 2006 through 2010. Locations with less than 75% temporal coverage (further indicated by an X) were not used in this study. Locations of contributing coastal HF radar sites and the location of NOAA's offshore mooring #46042 are marked by triangles and a circle, respectively. The HF radar locations are, from north-to-south, at Santa Cruz (SCRZ), Moss Landing (MLML), Naval Postgraduate School, Monterey (NPGS), Point Pinos (PPIN), Granite Canyon (GCYN), and Point Sur (PSUR). Note: At least, two additional HF radar sites located to the north of the mapping domain also contributed to vector current mapping within the domain. The bounding box in the southeast portion of the domain encloses the grid points whose kinetic energy is averaged together as an indication of the strength of the upwelling circulation. Representative depth contours (m) are also shown.

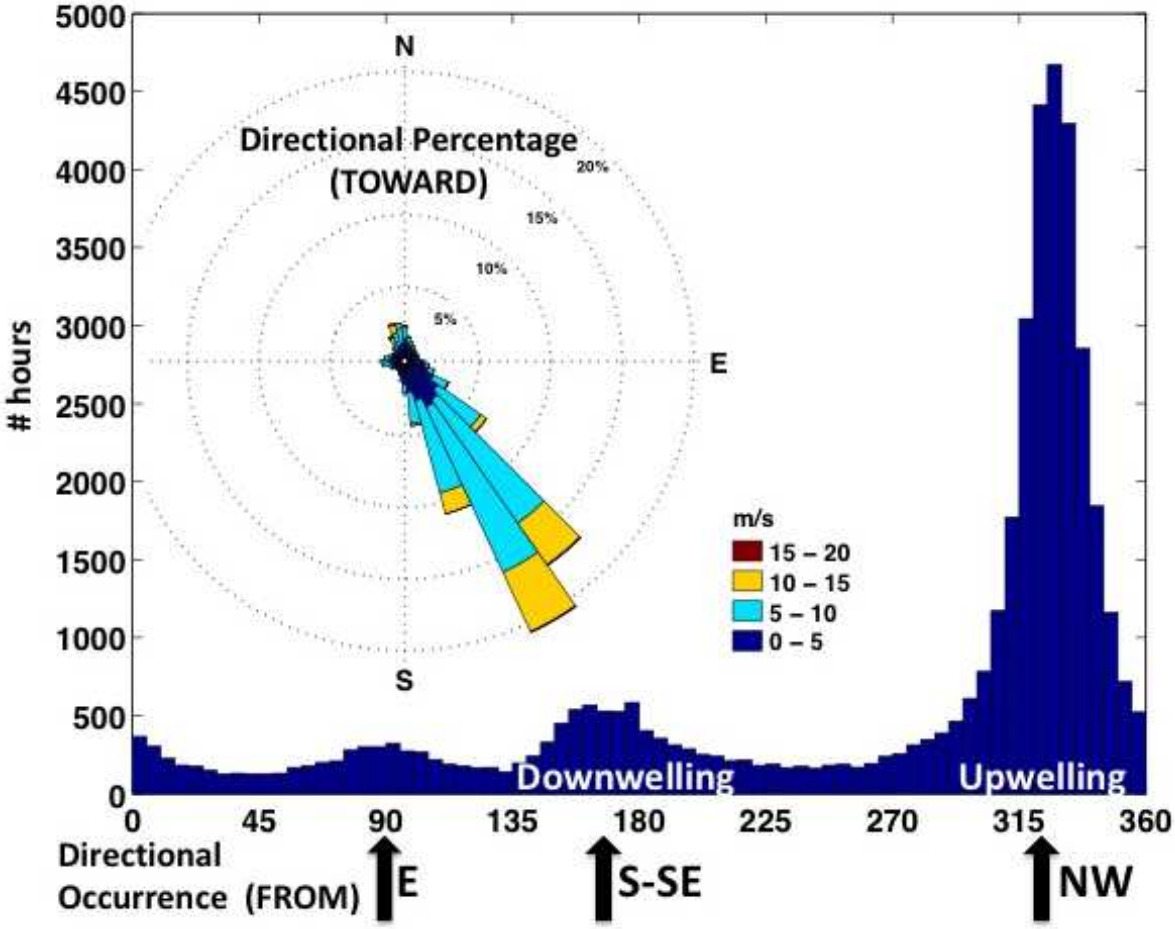

Figure 3. Directional statistics of 43,331 hourly wind velocity observations (out of a possible 43,824 hours) for the period 2006 through 2010 at NOAA's mooring #46042.

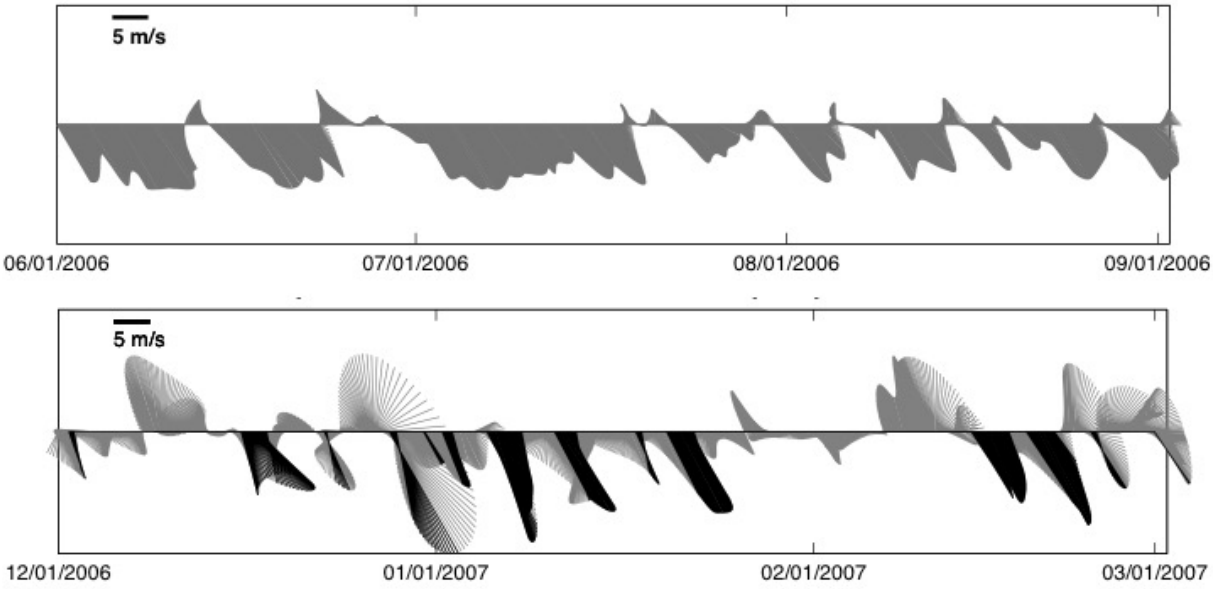

Figure 4. Sample summer (upper) and winter (lower) wind velocity at mooring #46042. Bold vectors in the winter data represent hours for which the speed exceeded 5.0 m/sec, the direction originated from between 280 degrees and 330 degrees, and these joint conditions were satisfied for, at least, the preceding 12 hours.

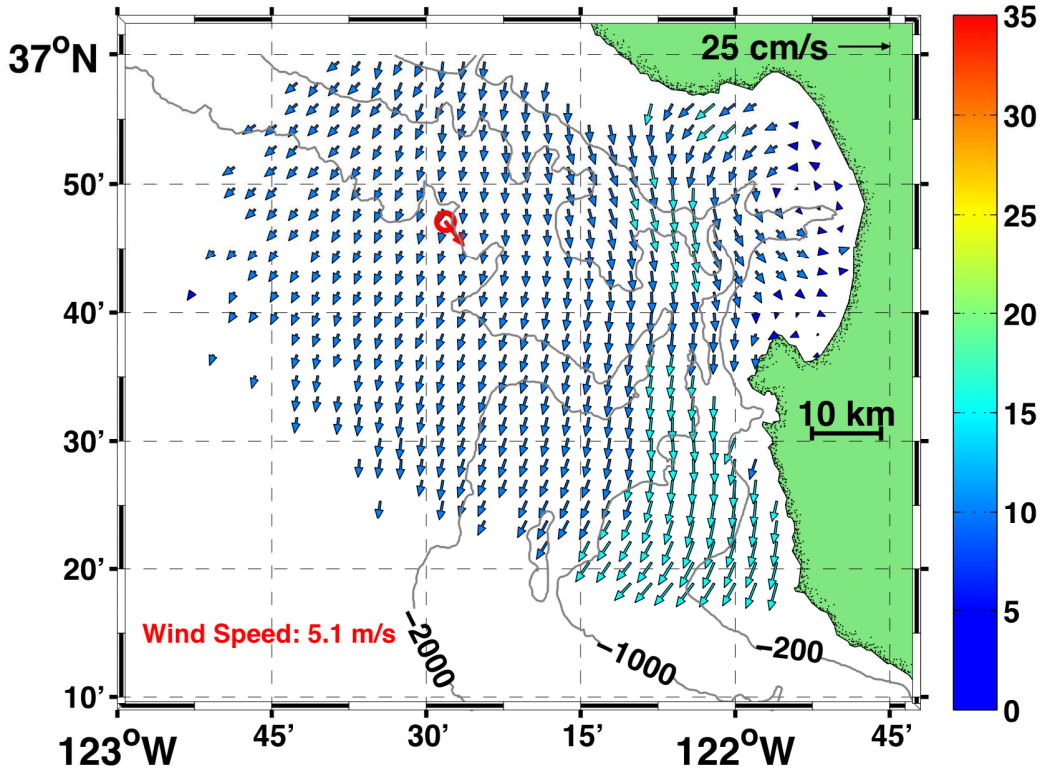

Figure 5. Summer (May-September) seasonal average surface currents and winds for 2006 through 2010. Representative depth contours (m) are also shown.

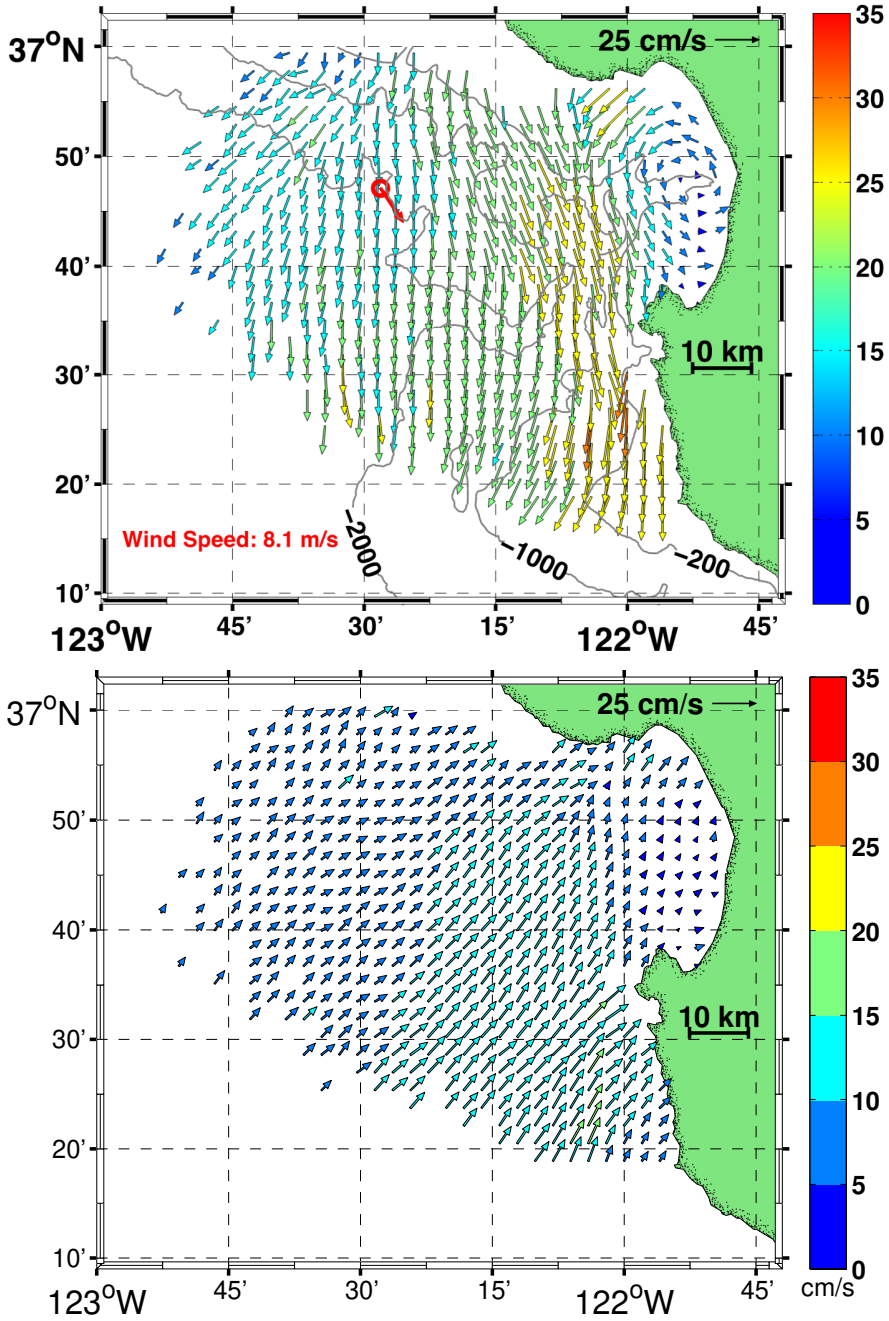

Figure 6. Upwelling circulation pattern for the summer months of May-September for 2006 through 2010 with wind speeds greater than 5.0 m/sec, wind direction between 280 degrees and 325 degrees, and these joint conditions having been met for between 204 hours to 216 hours (a spin up time of 8 ½ days). These upwelling-favorable wind conditions were matched 127 times in 12 events. The conditional average circulation pattern (upper) is paired with the standard error pattern (lower) assuming each event was independent. Representative depth contours (m) are also shown.

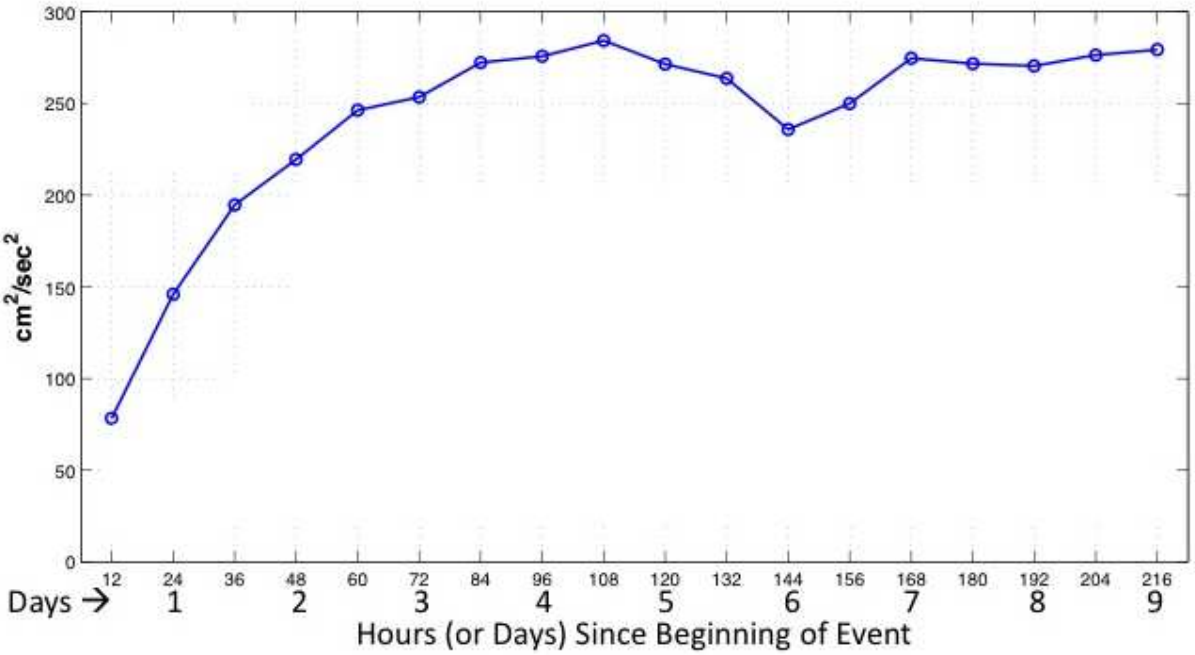

Figure 7. Mean kinetic energy within the sub grid area on Figure 2 as a function of time since the onset of upwelling-favorable winds.

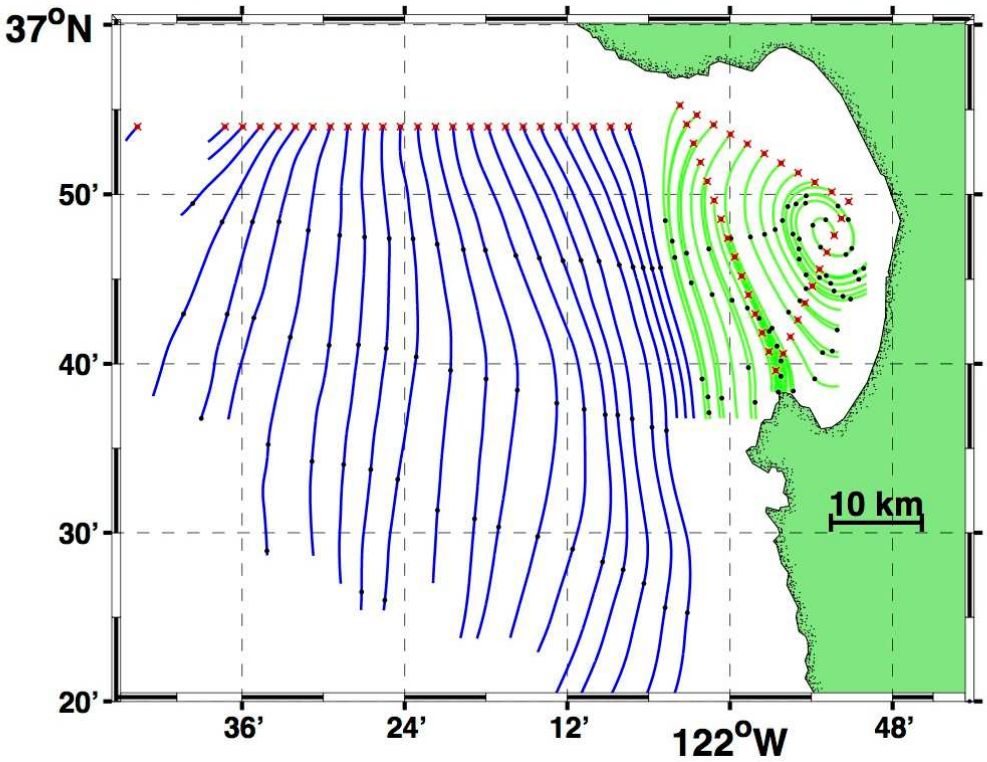

Figure 8. Frozen field visualization of the fully developed upwelling circulation pattern shown in Figure 5. X locations indicate the starting positions of offshore (blue) and inshore (green) surface particles.

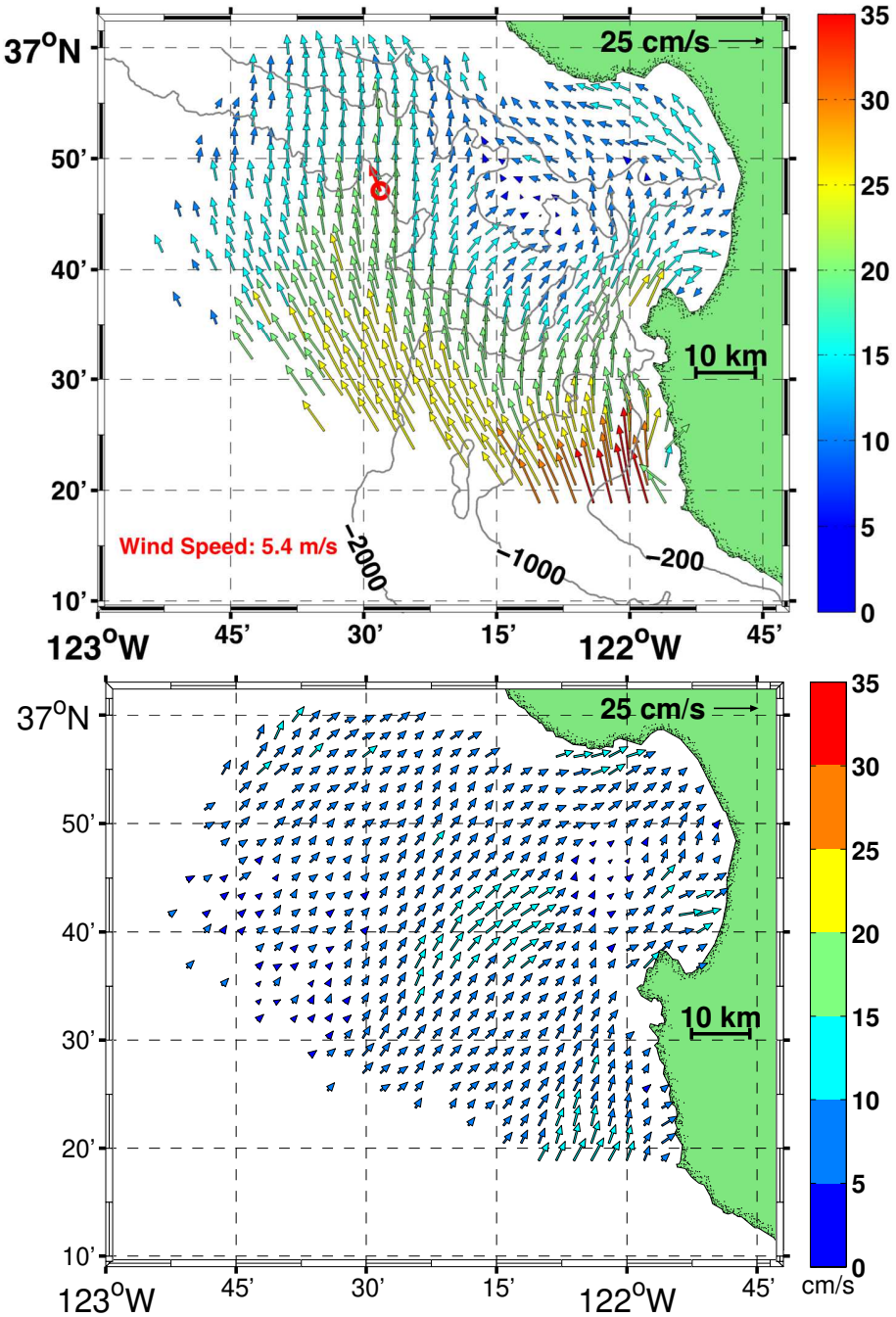

Figure 9. Circulation patterns during downwelling-favorable wind forcing with wind speeds >4 m/sec but <8 m/sec, wind direction from between 90 degrees and 150 degrees, and these joint conditions having been in place for, at least, 24 hours for the winter months of December, January, and February. These downwelling-favorable wind conditions were matched 57 times in 5 events. The conditional average circulation pattern (upper) is paired with the standard error pattern (lower) assuming each event was independent. Representative depth contours (m) are also shown.

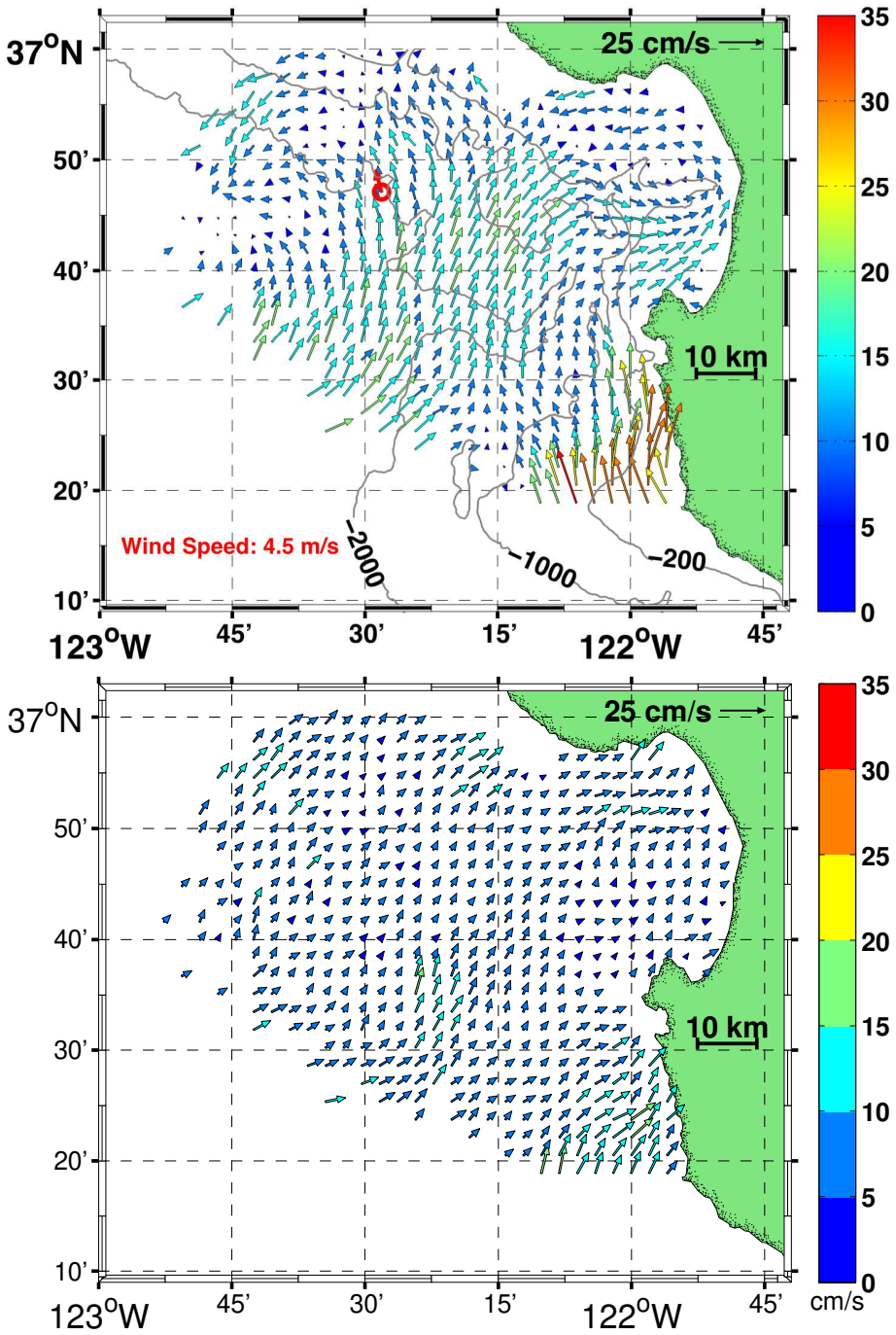

Figure 10. Circulation patterns during downwelling-favorable wind forcing with wind speeds >4 m/sec but <8 m/sec, wind direction from between 90 degrees and 135 degrees, and these joint conditions having been in place for, at least, 24 hours for the spring and summer months of May through September. The downwelling-favorable wind conditions were matched 65 times in 6 events. The conditional average circulation pattern (upper) is paired with the standard error pattern (lower) assuming each event was independent. Representative depth contours (m) are also shown.

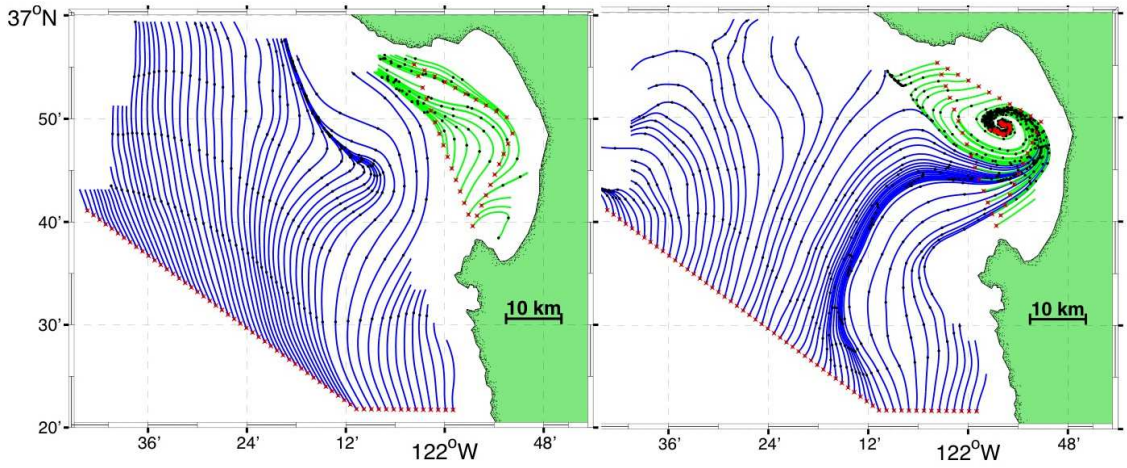

Figure 11. Frozen field visualization of the fully developed downwelling circulation patterns shown in Figure 9 and Figure 10 for winter (left) and spring-summer (right), respectively.

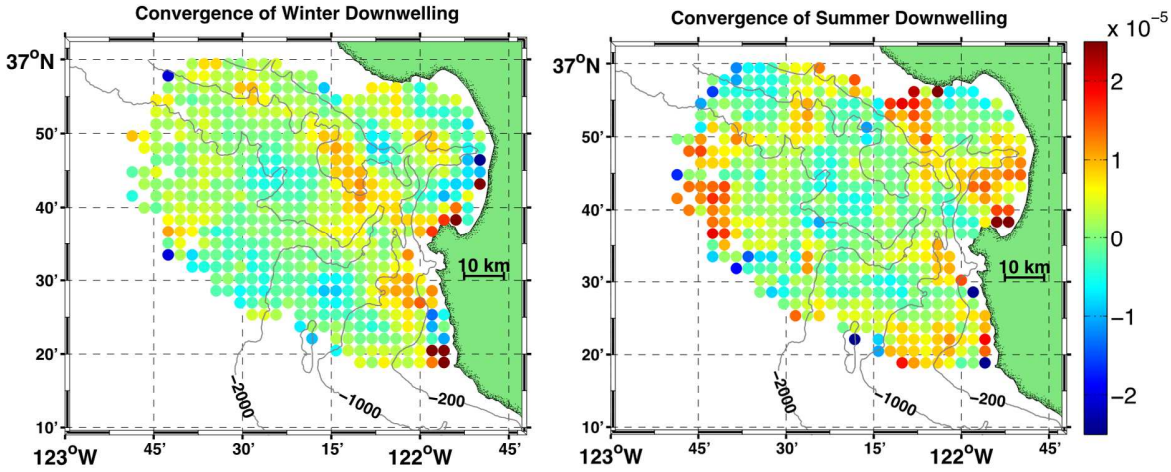

Figure 12. Convergence (sec^{-1}) for the wintertime (left) and summertime (right) downwelling circulation patterns from Figure 10. Representative depth contours (m) are also shown.

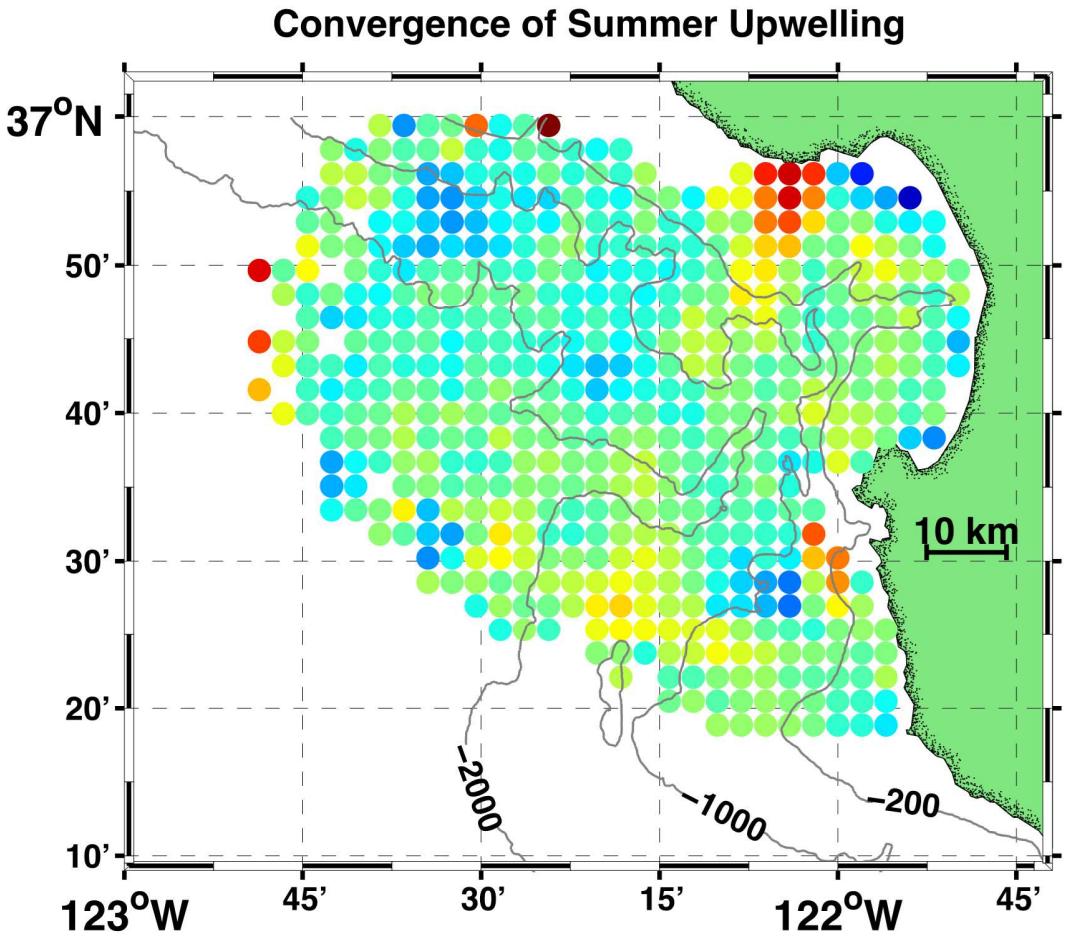

Figure 13. Convergence (sec^{-1}) for the fully developed summertime upwelling circulation pattern from Figure 6. Representative depth contours (m) are also shown.